ORIGINAL ARTICLE

Dynamical intrinsic functional architecture of the brain during absence seizures

Wei Liao · Zhiqiang Zhang · Dante Mantini · Qiang Xu · Gong-Jun Ji · Han Zhang ·
Jue Wang · Zhengge Wang · Guanghui Chen · Lei Tian · Qing Jiao · Yu-Feng Zang ·
Guangming Lu

Abstract Epilepsy is characterized by recurrent and
temporary brain dysfunction due to discharges of inter-
connected groups of neurons. The brain of epilepsy patients
has a dynamic bifurcation that switches between epileptic
and normal states. The dysfunctional state involves large-
scale brain networks. It is very important to understand the
network mechanisms of seizure initiation, maintenance,
and termination in epilepsy. Absence epilepsy provides a
unique model for neuroimaging investigation on dynamic
evolutions of brain networks over seizure repertoire. By
using a dynamic functional connectivity and graph theo-
retical analyses to study absence seizures (AS), we aimed
to obtain transition of network properties that account for
seizure onset and offset. We measured resting-state func-
tional magnetic resonance imaging and simultaneous
electroencephalography (EEG) from children with AS. We
used simultaneous EEG to define the preictal, ictal and
postictal intervals of seizures. We measured dynamic
connectivity maps of the thalamus network and the default
mode network (DMN), as well as functional connectome
topologies, during the three different seizure intervals. The
analysis of dynamic changes of anti-correlation between
the thalamus and the DMN is consistent with an inhibitory
effect of seizures on the default mode of brain function,
which gradually fades out after seizure onset. Also, we
observed complex transitions of functional network topol-
ogy, implicating adaptive reconfiguration of functional
brain networks. In conclusion, our work revealed novel
insights into modifications in large-scale functional con-
nectome during AS, which may contribute to a better

W. Liao and Z. Zhang contributed equally to this work.

W. Liao (✉) · G.-J. Ji · H. Zhang · J. Wang · Y.-F. Zang
Center for Cognition and Brain Disorders and the Affiliated
Hospital, Hangzhou Normal University, Hangzhou 310015,
China
e-mail: weiliao.wl@gmail.com

W. Liao · G.-J. Ji · H. Zhang · J. Wang · Y.-F. Zang
Zhejiang Key Laboratory for Research in Assessment of
Cognitive Impairments, Hangzhou 310015, China

W. Liao · Z. Zhang · Q. Xu · Z. Wang · Q. Jiao · G. Lu (✉)
Department of Medical Imaging, Nanjing Jinling Hospital,
Nanjing University School of Medicine, 305#, Eastern
Zhongshan Rd., Nanjing 210002, China
e-mail: cjr.luguangming@vip.163.com

D. Mantini
Department of Experimental Psychology, University of Oxford,
Oxford OX1, UK

D. Mantini
Department of Health Sciences and Technology, ETH Zurich,
8057 Zurich, Switzerland

G.-J. Ji
State Key Laboratory of Cognitive Neuroscience and Learning,
Beijing Normal University, Beijing 100875, China

G. Chen
Department of Neurology, Jinling Hospital, Nanjing University
School of Medicine, Nanjing 210002, China

L. Tian
Department of Neurosurgery, Jinling Hospital, Nanjing
University School of Medicine, Nanjing 210002, China

understanding the network mechanisms of state bifurcations in epileptogenesis.

Keywords Dynamic · Functional connectivity · Brain connectome · Absence seizure · fMRI

Introduction

Epilepsy is characterized by recurrent and temporary brain dysfunction due to discharges of interconnected groups of neurons. Our understanding of the network mechanisms of seizure initiation, maintenance, and termination during epilepsy is still limited (Kramer and Cash 2012; Richardson 2012). Absence epilepsy is a common type of generalized epilepsy in childhood (Chang and Lowenstein 2003). It is characterized by brief non-convulsive absence seizures (AS), and typical 2.5–4 Hz generalized spike-and-wave discharges (GSWDs), which can be detected by electroencephalography (EEG) (Blumenfeld 2005). These features make AS a unique model for neuroimaging investigation on dynamic evolutions of brain function over seizure repertoire (Kramer and Cash 2012).

Simultaneous EEG and functional magnetic resonance imaging (fMRI) is a multimodal imaging technique that is extremely valuable for epileptic activation localization and time-course analysis (Chaudhary et al. 2013). A number of studies have demonstrated dynamic blood-oxygen level dependent (BOLD) activation in the thalamus and deactivation in the brain regions of default mode network (DMN) (Raichle et al. 2001) corresponding to different seizure stages during AS (Bai et al. 2010; Benuzzi et al. 2012; Carney et al. 2010, 2012; Moeller et al. 2010). These findings may potentially relate to mechanisms of seizure generation and suspension of default mode of brain function in AS.

Moreover, epilepsy has been recently proposed to be a brain network disorder (Engel et al. 2013; Kramer and Cash 2012; Laufs 2012; Spencer 2002; Stefan and Lopes da Silva 2013). Through specific nodes and pathways, epileptic activity propagates from the source to wide brain regions, resulting in seizure occurrence and brain functional impairments (Gotman 2008). Functional connectivity (FC) MRI techniques were recently used for investigating brain networks in epilepsy (Liao et al. 2010; Vlooswijk et al. 2010, 2011; Zhang et al. 2011). Specifically, FC-MRI has contributed to link alterations intrinsic connectivity networks during AS to a set of specific cognitive impairments (Killory et al. 2011; Luo et al. 2011; Moeller et al. 2011; Yang et al. 2012).

Typical FC analyses measure the correlations of signals within a long period of time, thus providing a static pattern of brain activity coherences (Biswal et al. 1995). However, human brain connectivity is most likely to be time-dependent and dynamic, and to be related to ongoing rhythmic activity (Sporns 2011). Hence, dynamic FC techniques have been recently proposed to explore reconfiguration of brain networks (Allen et al. 2012; Chang and Glover 2010; de Pasquale et al. 2010; Handwerker et al. 2012; Hutchison et al. 2012; Kang et al. 2011; Lee et al. 2013), and have proved to be especially valuable when investigating the variability of the large-scale brain connectome across different states (Bassett et al. 2011; Fornito et al. 2012).

Aiming at contributing to a better understanding to the evolution of seizures at a network level, we conducted a simultaneous EEG-fMRI study on patients with AS. We used EEG to define preictal, ictal, and postictal stages of AS, and we then applied a dynamic analysis of FC-MRI across these three stages. Accordingly, we revealed novel insights into the mechanisms underlying dynamics of large-scale brain networks related to the initiation, maintenance and termination of AS.

Method

Participants

A total of 15 patients with typical childhood absence epilepsy (11 females, all right-handed; age [mean ± SD]: 8.06 ± 3.15 years) were recruited from 2009 to 2013 at Jinling Hospital, Nanjing University School of Medicine. Written informed consent was obtained from all participants. The study was approved by the local medical ethics committee at Jinling Hospital, Nanjing University School of Medicine. Patients met the following diagnosis criteria: (a) clinical diagnosis of childhood absence epilepsy was established according to the International League against Epilepsy (ILAE) classification; (b) EEG with typical bilateral, synchronous 2.5–4 Hz GSWDs; (c) no additional seizure types, such as myoclonic, tonic–clonic, or partial seizures; and (d) no focal abnormality in routine structural MRI examinations (Table 1).

EEG-fMRI data acquisition

All patients underwent simultaneous EEG-fMRI recording. Functional and structural imaging was scanned using a Siemens Trio 3T scanner at Jinling Hospital, Nanjing, China. Foam padding was used to minimize head motion for all subjects. Functional images were acquired using a single-shot, gradient-recalled echo planar imaging sequence (repetition time = 2,000 ms, echo time = 30 ms and flip angle = 90°). Thirty transverse slices (field of view = 240 × 240 mm^2, in-plane matrix = 64 × 64,

Table 1 Demographic and clinical information of patients

Patient	Sex/age (years)	Onset age (years)	Medication	Session	No. of AS (duration, s)	No. of selected seizures (durations)	All events (duration, s)	Frequency of GSWDs (Hz)
1	F/12	9	None	2	5 (119)	2 (60)	119	2.5–3.5
2	M/9	6	None	2	1 (9)	1 (9)	9	3–4
3	F/18	10	SV	2	2 (14)	2 (14)	30	3–4
4	F/7	7	SV	2	19 (229)	8 (104)	229	3–3.5
5	F/8	6	SV	2	1 (12)	1 (12)	12	2.5–3.5
6	M/7	5	SV	2	1 (16)	1 (16)	52	3–4
7	F/5	4	None	2	6 (36)	6 (36)	36	2.5
8	F/11	9	None	2	1 (14)	1 (14)	14	3–4
9	M/7	5	SV, LTG, LEV	2	3 (34)	3 (34)	73	3.5
10	F/6	4	SV, LTG, LEV	2	4 (37)	2 (28)	37	3–3.5
11	F/10	3	SV, LTG,	2	1 (15)	1 (15)	55	3–4

F female, *M* male, *SV* sodium valproate, *LTG* lamotrigine, *LEV* levetriacetam, *AS* absence seizures, *GSWDs* generalized spike-and-wave discharges

slice thickness = 4 mm, interslice gap = 0.4 mm, voxel size = $3.75 \times 3.75 \times 4$ mm^3), aligned along the anterior commissure–posterior commissure line were acquired. In each session, a total of 505 volumes were collected, resulting in a total scan time of 1,010 s. For each subject, 2–5 sessions were acquired. Subjects were instructed simply to rest with their eyes closed, not to think of anything in particular, and not to fall asleep. Subsequently, 3D T1-weighted anatomical images were acquired in the sagittal orientation using a magnetization-prepared rapid acquisition gradient-echo sequence (repetition time = 2,300 ms, echo time = 2.98 ms, flip angle = 9°, field of view = 256×256 mm^2, matrix size = 256×256, slice thickness = 1 mm, no interslice gap, voxel size = $1 \times 1 \times 1$ mm^3 and 176 slices) on each subject.

During fMRI acquisition, EEG data was continuously recorded through a 10/20 systems with 32 Ag/AgCl electrodes attached to the scalp with conductive cream. Three EOG/ECG channels were simultaneously recorded. Twenty-nine EEG electrodes were connected to a BrainAmp amplifier (Brain Products, Germany), with a sampling rate of 5,000 Hz. The amplifier was connected to the recording computer outside the scanner room via a fiber optic cable.

Typical ictal seizure behaviors were monitored by a camera in the scanner. Clinical behavioral of absences included eyelid fluttering, staring and mild myoclonic jerks. Specifically, mild myoclonic jerks induce head movement artifacts, which are reflected in both EEG and fMRI data. If excessive movements were detected during data collection, the acquisition run was aborted and then started again.

EEG analysis

The EEG was processed offline to filter out MR artifacts and to remove ballistocardiogram artifacts (Brain Vision Analyzer 2.0, Germany). Onset and end time of epileptic discharges (typical 2.5–4 Hz GSWDs) were tagged and classified by an experienced neurologist and electroencephalographer, according to both spatial distribution and morphology. If no spike-series was found in a single session, this fMRI data was excluded from subsequent analyses.

fMRI data preprocessing

Functional images preprocessing was carried out using the DPARSF (http://www.restfmri.net) and SPM8 (http://www.fil.ion.ucl.ac.uk/spm) toolkit. Functional images, after exclusion of the first 5 images to ensure steady-state longitudinal magnetization, were initially corrected for temporal differences and head motion. No translation or rotation parameters in any given data set exceeded ±3 mm or ±3°. We then co-registered individual 3D T1-weighted anatomical image to functional images. The 3D T1-weighted anatomical images were segmented (grey matter, white matter and cerebrospinal fluid). Then, a nonlinear spatial deformation was calculated from the grey matter images to a grey matter template in Montreal Neurological Institute (MNI) space. This transformation was then applied to the functional images, which were resliced at a resolution of $3 \times 3 \times 3$ mm^3 and spatially smoothed with an 8-mm full-width half-maximum isotropic Gaussian kernel. No spatial smoothing was applied for functional connectivity network analysis, to avoid introducing artificial local spatial correlations, as previously suggested (Salvador et al. 2005; Zhang et al. 2011; Zuo et al. 2012).

GSWDs-related BOLD activity

Analysis of functional images was performed in SPM8 toolkit by means of a general liner model, using GSWDs

convolved with a canonical hemodynamic response function as regressors (Bai et al. 2010; Gotman et al. 2005). The epochs of GSWDs were represented as variable duration blocks beginning at the onset of seizure and ending upon GSWD cessation. Motion realignment parameters were also included as covariates of no interest. For group analysis, a second-level random effects model (one sample *t* test) was performed to determine regions showing significant fMRI changes among patients. We also applied a false discovery rate (FDR) procedure to correct for multiple comparisons (Genovese et al. 2002).

Analysis of dynamic FC map

We estimated dynamic FC changes before, during, and after seizures. Before this procedure, BOLD data were processed to attenuate the contribution of six head motion parameters, averaged signals from cerebrospinal fluid and white matter, and the global brain signal (Fox et al. 2005); next, the time series were band-pass filtered (0.01–0.08 Hz). Two specific volumes of interest (VOIs) were selected as seeds for FC analysis, based on regions showing the GSWDs-related BOLD activation and deactivation. These VOIs were bilateral thalamus and posterior cingulate cortex/precuneus (PCC/PCUN) (Table 2).

Subsequently, we evaluated dynamic FC changes using a sliding-window correlation approach (Hutchison et al. 2012) (see Fig. 1 for a schematic of the sliding-window approach). We calculated correlation maps between the time series derived from the seeds and all other brain voxels for a sliding window of 50 volumes (100 s). We also investigated the effect of other window lengths (60 and 200 s). For each sliding window, we obtained a correlation map, which was then converted to z-scores using the Fisher r-to-z transformation. The window was then shifted by one volume (2 s) and a new correlation map was calculated. This approach permitted to estimate functional connectivity over time, in temporal windows such as: 1–50, 2–51, 3–52,…, 451–500 (Kiviniemi et al. 2011). Since the time series were composed of 500 volumes, this procedure yielded 451 correlation maps (Handwerker et al. 2012). The dynamic correlation maps were separated into preictal (time before seizure onset), ictal, and postictal (time after seizure end) time periods by using information from EEG recordings. These three periods covered a time range from −22 to +32 s relative to seizure onset. The ictal period of each seizure was scaled to the mean seizure duration (12.64 s in our data). For subsequent group analysis, we resampled the number of FC maps and matrices to account for different seizure durations (Bai et al. 2010). Specifically, if the ictal period was longer or shorter than mean seizure duration, the related FC maps and matrices were down- and up-sampled to keep constant their number across different seizures (this number was 6, since the mean size duration was 12.64 s). In contrast, the preictal (22 s duration) and postictal (22 s duration) data were not resampled, but just aligned in time across seizures. This was done by lining up the seizure onset times for preictal data, and by lining up the seizure offset times for postictal data, as in previous studies (Bai et al. 2010).

We used a one-way within-subject analysis of variance (ANOVA) ($P < 0.05$, FDR-corrected) to determine

Table 2 Significant clusters of GSWDs-related BOLD activation and deactivation

Region	Hem.	Activation/ deactivation	Peak coordinates MNI (x, y, z)	Cluster size (voxels)	T value
THA[a]	L/R	Activation	−12, −27, 12	382	11.31
Ventricle	L	Activation	−21, 30, 6	25	6.94
	R	Activation	21, 33, 6	40	6.42
PCC/PCUN[b]	L/R	Deactivation	9, −51, 24	561	−10.03
MTG	L	Deactivation	−57, −24, −9	88	−6.03
	R	Deactivation	60, −3, −24	423	−8.86
ITG	L	Deactivation	−51, 6, −33	81	−7.31
PHIP	L	Deactivation	−27, −30, −15	83	−6.08
	R	Deactivation	27, −21, −21	47	−6.16
CAU/PUT	L	Deactivation	−15, 9, −3	82	−6.68
	R	Deactivation	15, 12, −3	95	−7.44
ACC	L/R	Deactivation	−3, 39, 6	54	−5.33
MCC	L/R	Deactivation	3, −27, 39	56	−5.87
AG	L	Deactivation	−42, −57, 24	264	−6.55
	R	Deactivation	54, −63, 24	209	−7.37
Pons	L/R	Deactivation	9, −24, −36	125	−9.24

THA thalamus, *PCC/PCUN* posterior cingulate cortex/precuneus, *MTG* mesial temporal gyrus, *ITG* inferior temporal gyrus, *PHIP* parahippocampus, *CAU* caudate nucleus, *PUT* putamen, *ACC* anterior cingulate cortex, *MCC* median cingulate cortex, *AG* angular gyrus

[a] Showing GSWDs-related BOLD activation considering as VOI

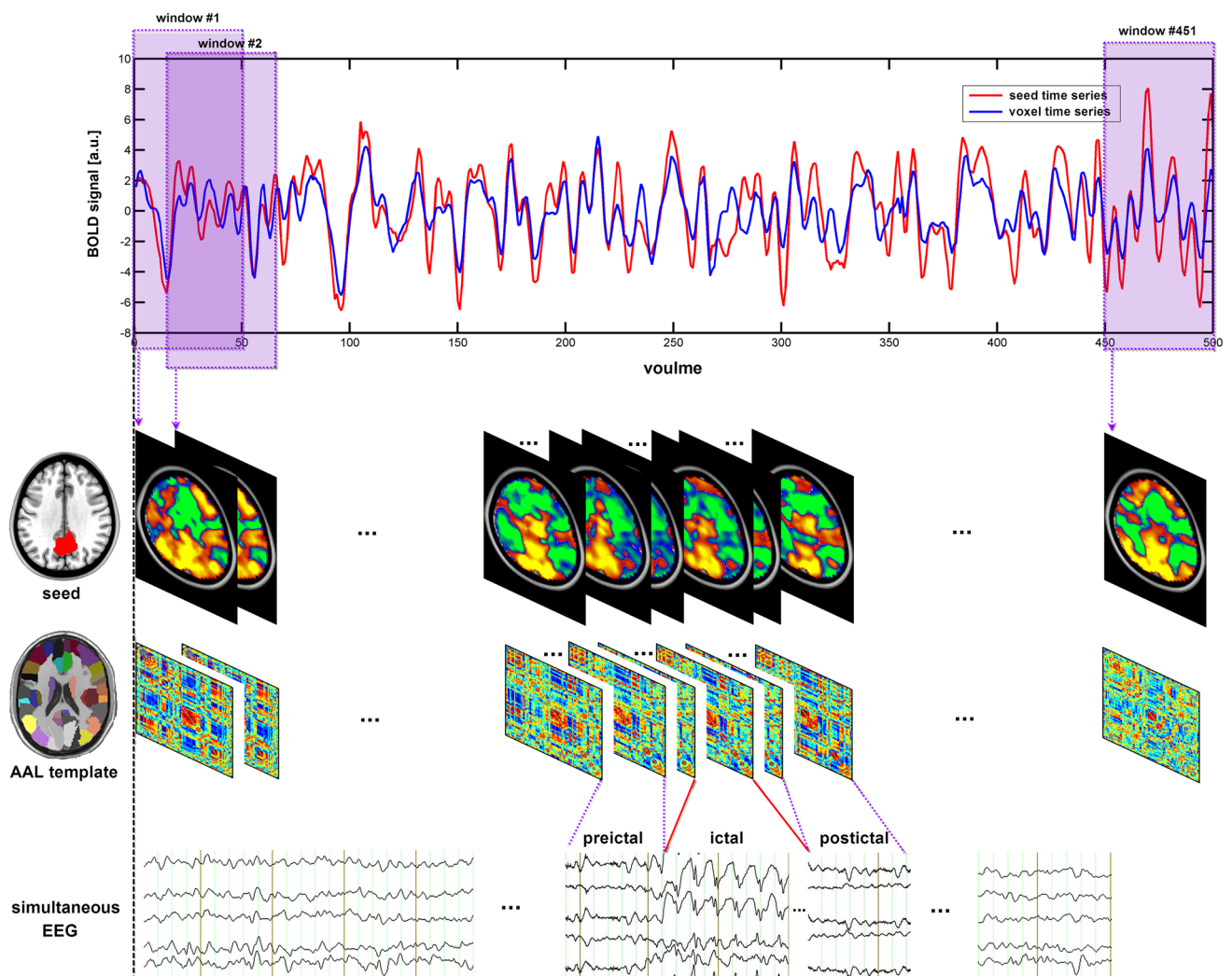[b] Showing GSWDs-related BOLD deactivation considering as VOI

Fig. 1 Schematic of the sliding-window FC approach. The time series of the seed (*red line in the top row*) and of a representative brain voxel (*blue line in top row*) were correlated using a sliding-window of 50 volumes (100 s). For window #1, which is defined on volumes 1–50, the correlation between the time series of the seed and of all brain voxels is calculated, resulting in the creation of a correlation map. The window was then shifted by one volume and a new correlation map was calculated (e.g., window #2, defined on volumes 2–51). This procedure allowed the estimation of FC over time. Since the time series had 500 volumes in our data, we calculated 451 correlation maps in total (see *second row* in the figure). Similarly, for each sliding-window of 50 volumes, we compared by temporal correlation the time series extracted from a set of regions of interest (*ROIs*) covering the whole brain. This resulted in a set of 451 temporal correlation matrices (see *third row* in the figure). The dynamic FC maps and matrices for the preictal (time period before seizure onset), ictal, and postictal (time period after seizure offset) were selected using information from simultaneously collected EEG data (see *bottom row*)

significant changes in the correlation maps (after Fisher r-to-z transform) across the intervals for the entire set of seizures.

Moreover, to test the reliability of the dynamic FC results, we carried out a split-half analysis (He et al. 2009; Zhang et al. 2011). Specifically, we divided the total 28 seizures into two subgroups (14 seizures for each subgroup). For each subgroup, the seed-based dynamic FC analysis was calculated as in the whole-group analysis. Then, we performed a one-way within-subject ANOVA on the functional connectivity maps of each subgroup, and we assessed the spatial correspondence between the resulting ANOVA maps. Furthermore, we tested the consistency of these findings by repeating a slip-half analysis 100 times, dividing each time the 28 seizures into two different groups of 14 seizures. For each split-half analysis, we performed a one-way within-subject ANOVA, and we then created a consistency map showing the frequency with which the brain regions were found to be significant in the ANOVA test.

Dynamic functional connectome analysis

The whole cerebral cortex was parcelled into 90 anatomical ROIs using the automated anatomical labeling (AAL) template (Tzourio-Mazoyer et al. 2002). This parcellation scheme will be referred to as AAL-90. A list of anatomical labels of the nodes is presented in the Online Resource Table 1. Considering that the range of nodal scale and the difference in template parcellations may impact on the results of network analysis (Hagmann et al. 2010; Wang et al. 2009), we also used a high-resolution parcellation scheme with 512 ROIs (Hagmann et al. 2008). Specifically, we generated 512 ROIs of approximately identical size across both hemispheres by subdividing each region in the low-resolution AAL-90 template into a set of subregions. This parcellation scheme will be referred to as AAL-512 (Zhang et al. 2011). These two types of parcellation schemes were used in parallel for network analyses, for a cross-validation of our results. As mentioned above, we obtained regional BOLD time series by averaging time series across voxels in each ROI using non-smoothed functional images. The time series were preprocessed as for seed-based FC analysis. For each sliding window, we obtained a temporal correlation matrix (90×90 or 512×512) whose elements (r_{ij}) are Pearson correlation coefficients between every pair of ROIs. Since the time series included 500 volumes, we obtained 451 temporal correlation matrices in total. Again, the correlation matrices within the ictal period were resampled to equalize the seizure duration, whereas those within the preictal (22 s) and postictal (22 s) period were not scaled but just aligned (Bai et al. 2010). Individual elements of r_{ij} were subjected to statistical testing for the construction of weighted functional connectivity networks. The value of r_{ij} that was not significant at the corrected level ($P < 0.05$, FDR-corrected) was set to zero, or it was kept otherwise.

Graph theoretical analyses were carried out on each network for the preictal, ictal and postictal periods using the Brain Connectivity Toolbox (http://www.brain-connectivity-toolbox.net) (Rubinov and Sporns 2010). We calculated both overall topology and nodal characteristic. The overall topologies included: small-world property (Sigma), which quantifies simultaneous global and local parallel information processing in brain networks (Bassett and Bullmore 2006); weighted clustering coefficient (C_{net}^{w}), which quantifies the local interconnectivity or cliquishness of the network, and normalized weighted clustering coefficient (Gamma); weighted characteristic shortest path length (L_{net}^{w}), which quantifies the ability for parallel information propagation, and normalized weighted characteristic shortest path length (Lambda); the nodal degree (S_{u}^{w}) and the total connection strength in network (S_{net}^{w}),

which quantifies the extent to which a node is relevant to the graph, and the sum of the weights of all the connections of the network, respectively. To determine how the overall network topology evolved in time, we applied a one-way within-subject ANOVA on overall topologies across intervals over the entire collection of seizures. Furthermore, we performed two-sample t tests between values for the preictal, ictal and postictal periods.

Projection of volumes to cortical surface

For visualization purpose, group-level GSWDs-related BOLD activity map and dynamic FC maps were projected from the volumes to the individual cortical surfaces and then registered to the ICBM152 brain surfaces using Freesurfer (http://surfer.nmr.mgh.harvard.edu/). The surface maps were visualized using BrainNet Viewer (http://www.nitrc.org/projects/bnv/). Dynamic functional connectome results were also visualized with BrainNet Viewer. In this case, nodes were positioned according to the ROIs' centroid stereotaxic coordinates and were colored according to six anatomical subsystems. Hub nodes were indicated with larger size. Furthermore, edges are coded according to their connection weights.

Results

We collected simultaneous EEG-fMRI data from 15 children with AS, over a time period of about 16 min each. Of these 15 patients together, 11 patients had AS and therefore contributed data for our analysis. We identified 44 seizures in total (Table 1). To avoid confounding effects in sliding-window length for FC/brain network analyses, we selected only the GSWDs seizures with discharges longer than 6 s and with minimum interval of 20 s between the end of the last GSWDs and the beginning of the next GSWDs. This criterion led us to the selection of 28 seizures (duration: mean ± SD = 12.64 ± 9.46 s), which were used in subsequent analyses (see Table 1; Fig. 2 for information on patients and their contribution in terms of seizure number). Our statistical analyses revealed no significant difference of seizure duration among patients (Kruskal–Wallis statistic value was 16.61, $P = 0.0834$).

Brain activity during GSWDs

We observed BOLD increases in the bilateral thalamus, as well as decreases in the bilateral angular gyrus, temporal cortex, parahippocampus, basal ganglia and PCC/PCUN (Fig. 3; Table 2), which largely belong to the DMN (Fox et al. 2005; Raichle et al. 2001). The thalamus network and the DMN were previously shown in studies of BOLD
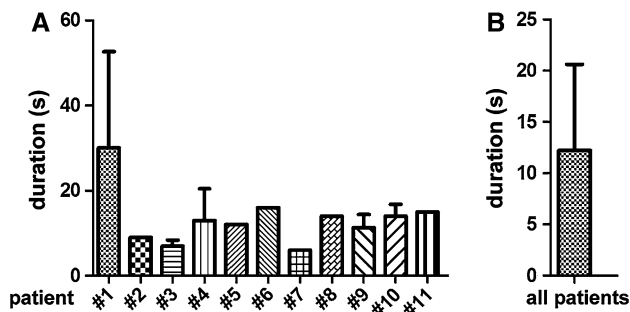
Fig. 2 The distribution of the duration of the seizures in individual patients and in all patients. The *bar* plot shows, for each single patient (**a**) and for all patients together (**b**), the duration of the detected seizures. The *error bars* indicate the standard deviation (*SD*)
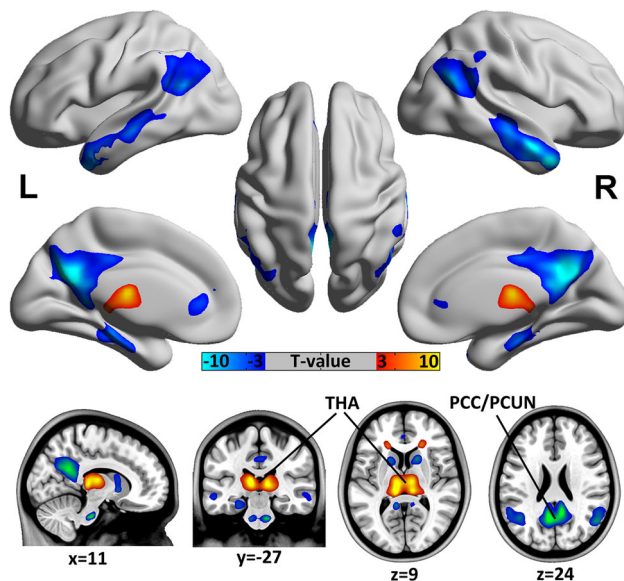

Fig. 3 GSWDs-related BOLD activation and deactivation in absence seizures. A second-level random effects analysis revealed significant BOLD activation (*warm color*) and deactivation (*cool color*) (FDR-corrected height threshold $P < 0.05$, and extent threshold k = 5 voxels). The results are presented on inflated surface maps (*Upper*) and axial maps (*Lower*). *THA* thalamus, *PCC/PCUN* posterior cingulate cortex/precuneus, *L* left hemisphere, *R* right hemisphere

changes related to GSWDs (Archer et al. 2003; Gotman et al. 2005; Moeller et al. 2008a, b).

Dynamic FC maps using the thalamus as seed

The FC maps of patients were characterized by negative correlations between the thalamus and DMN regions (Fig. 4a). When we compared the FC maps from the thalamus across all subjects and seizures within the preictal, ictal, and postictal intervals, we found that significant changes were located within the subcortical regions [bilateral thalamus, caudate nucleus (CAU), putamen (PUT)], and cortical regions mainly encompassing the

DMN [(PCC/PCUN), inferior parietal lobule (IPL), hippocampus, angular gyrus, medial prefrontal cortex] (one-way within-subjects ANOVA, $P < 0.05$, FDR-corrected) (Fig. 4b). Moreover, FC between thalamus and the bilateral basal ganglia (CAU, PUT), PCC/PCUN and IPL showed anti-correlation in the preictal and ictal periods and positive correlation in the postictal period (Fig. 4c).

Dynamic FC using PCC/PCUN as seed

We investigated dynamic FC using the PCC/PCUN as seed. In line with previous studies (Fox et al. 2005), we found positive correlations between the PCC/PCUN and regions of the DMN, and negative correlations between the PCC/PCUN and regions of task-positive networks. Moreover, the bilateral thalamus showed anti-correlations with the PCC/PCUN in patients with AS (Fig. 5a). We then compared the FC maps for all subjects and seizures within preictal, ictal, and postictal intervals. Significant changes in FC maps across periods were located at the bilateral CAU, cuneus, pre/post-central gyrus, and the right thalamus and fusiform gyrus (one-way within-subjects ANOVA analysis, $P < 0.05$, FDR-corrected) (Fig. 5b). Specifically, the bilateral CAU showed positive correlation with PCC/PCUN within the preictal period and decreased over time, finally showing anti-correlation during the postictal period (Fig. 5c). As absence seizures evolved, the right thalamus had an increase in correlation with the PCC/PCUN (Fig. 5c).

Reproducibility of dynamic FC findings

We assess the reproducibility of our findings by using a split-half analysis. Specifically, we divided the seizures in two subgroups and we compared the results of each of them. With either the thalamus or the PCC/PCUN as seed, our split-half analysis showed similar dynamic FC patterns, although less reliable than those obtained from the whole group (Fig. 6). When we investigated dynamic FC using thalamus as seed, the common significant changes in FC were located in the bilateral CAU, PUT and thalamus (Fig. 6a). For the PCC/PCUN as seed, the common significant changes in FC were in bilateral CAU, PUT and right THA (Fig. 6b).

Dynamic large-scale functional connectome

We used a sliding-window seed-based FC analysis to study brain dynamics of seizure generation, maintenance and termination in AS patients. As an exploratory analysis, we were also interested in how the large-scale functional connectome evolves across time, and how time evolution reflects changes related to seizure periods. Accordingly, we
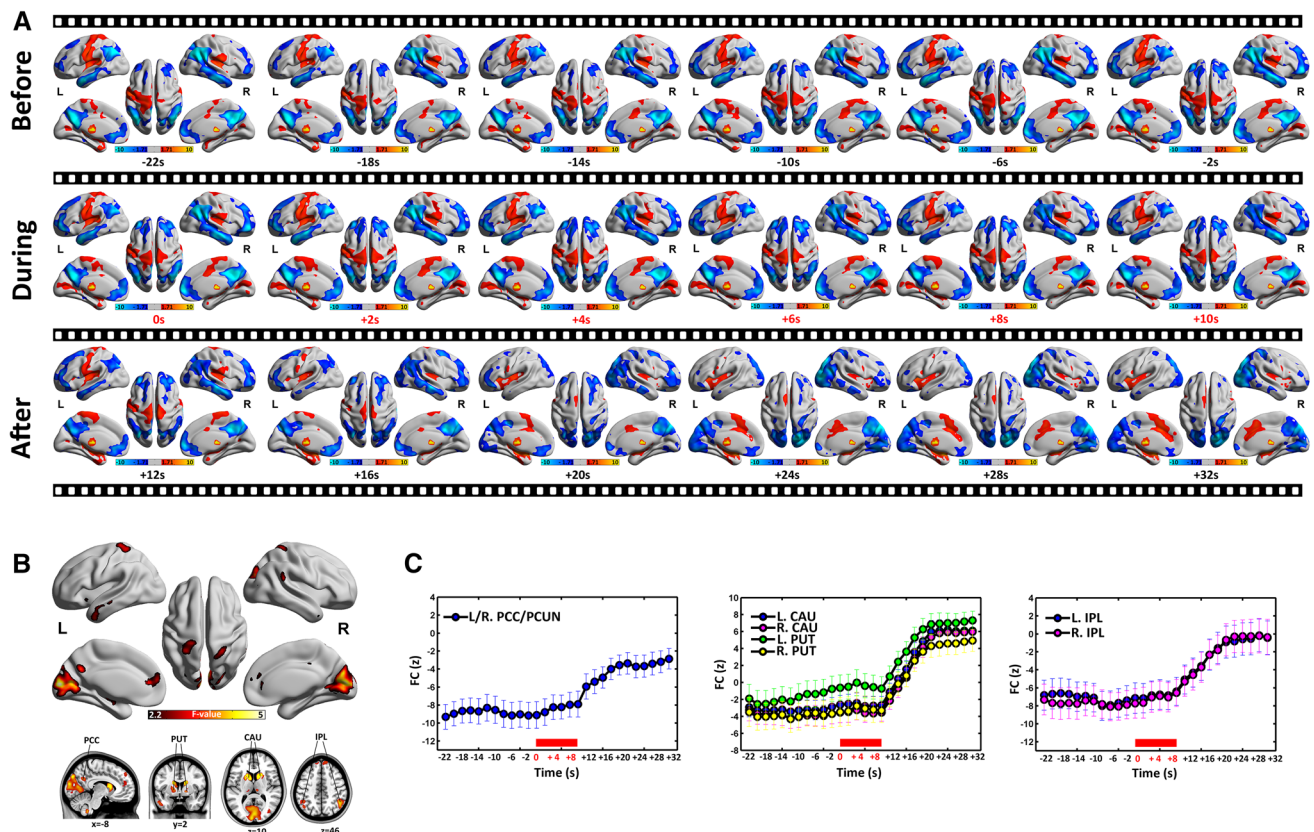
Fig. 4 Dynamic changes of the thalamus network during AS. **a** Significant positive (*warm color*) and negative (*cool color*) correlations were derived from one-sample *t* test (uncorrected heighted threshold $P < 0.05$, and extend threshold k = 5 voxels). The results are presented on inflated surface maps for preictal (*Upper*), ictal (*Middle*) and postictal (*Lower*) periods from −22 to +32 s, relative to seizure onset. **b** Significant change of the thalamus network across the preictal, ictal, and postictal intervals (one-way within-subject ANOVA, FDR-corrected height threshold $P < 0.05$,

and extent threshold k = 5 voxels). Significant network changes (*warm color*) are presented on inflated surface maps (*Upper*) and axial maps (*Lower*). **c** Mean FC strength (*Z* value) time courses in six anatomical clusters (PCC/PCUN, CAU, PUT and IPL). *Error bars* represent SEM across seizures. The mean seizure duration is shown in the *red box*. *PCC/PCUN* posterior cingulate cortex/precuneus, *CAU* caudate nucleus, *PUT* putamen, *IPL* inferior parietal lobule, *L* left hemisphere, *R* right hemisphere

measured FC between areas defined in either the low-resolution AAL-90 or high-resolution AAL-512 parcellation scheme, for each interval from the preictal, ictal, and postictal periods (Figs. 7, 8). For the low-resolution AAL-90 parcellation, a one-way within-subjects ANOVA analysis across all intervals showed different overall topologies on total connection strength ($F = 3.184$, $P = 0.0000$), overall clustering coefficient ($F = 3.992$, $P = 0.0000$) and overall characteristic shortest path length ($F = 4.431$, $P = 0.0000$). No significant change was found in the small-worldness index ($F = 1.280$, $P = 0.1560$). We observed larger total connection strength ($T = 2.441$, $P = 0.0214$) and clustering coefficient ($T = 2.946$, $P = 0.0065$) and decreased shortest path length ($T = -2.954$, $P = 0.0064$) between ictal and postictal periods. When we used the high-resolution AAL-512 parcellation, we obtained findings consistent to those of the AAL-90 parcellation, for total connection strength ($F = 6.358$, $P = 0.0000$), overall clustering coefficient ($F = 8.070$,

$P = 0.0000$) and overall characteristic shortest path length ($F = 10.663$, $P = 0.0000$). However, a one-way within-subjects ANOVA analysis on normalized weighted characteristic shortest path length (Lambda) showed different values across intervals ($F = 4.854$, $P = 0.0000$), and was specifically lower between ictal and postictal periods ($T = -2.664$, $P = 0.0128$).

FC during nondischarge periods

Previous studies suggested the presence of distinct FC patterns between GSWDs and nondischarge states in IGE (Luo et al. 2012; Moeller et al. 2011; Yang et al. 2012). To test this hypothesis, we selected nondischarge periods (no GSWDs detected during a given session) and randomly tagged intervals as they were moments of seizure onset. We repeated our one-way within-subject ANOVA on dynamic FC maps for nondischarge periods, and we found no significant difference neither with PCC/PCUN nor
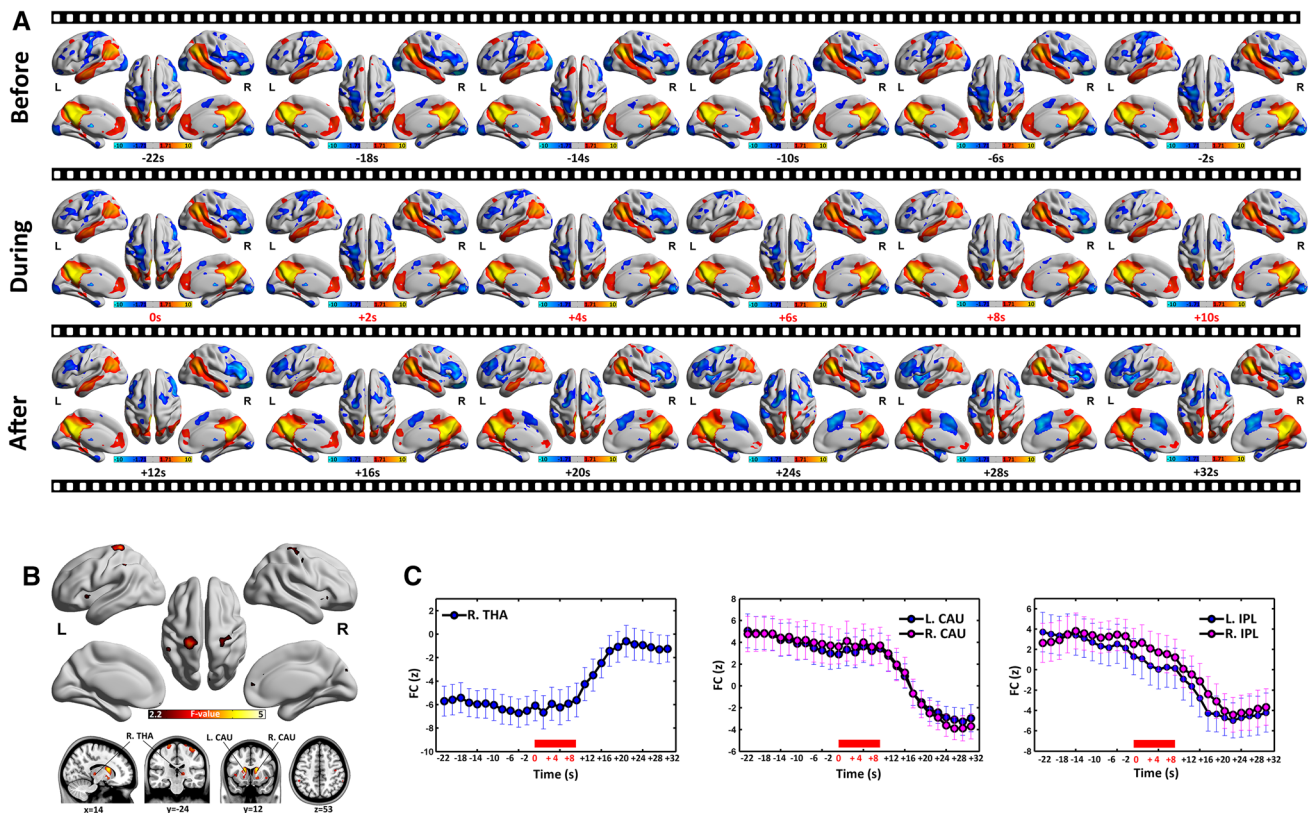
Fig. 5 Dynamic changes in the DMN during AS. **a** Significant positive (*warm color*) and negative (*cool color*) correlations were derived from one-sample *t* test (uncorrected heighted threshold $P < 0.05$, and extend threshold k = 5 voxels). The results are presented on inflated surface maps for preictal (*Upper*), ictal (*Middle*) and postictal (*Lower*) periods from −22 to +32 s, relative to seizure onset. **b** Significant change of the DMN across the preictal, ictal, and postictal intervals (one-way within-subjects ANOVA analysis, FDR-corrected height threshold $P < 0.05$, and extent threshold k = 5 voxels). Significant network changes (*warm color*) are presented on inflated surface maps (*Upper*) and axial maps (*Lower*). **c** Mean FC strength (Z value) time courses in five anatomical clusters (THA, CAU, and IPL). *Error bars* represent SEM across all seizures. The mean seizure duration is shown in the *red box*. *THA* thalamus, *CAU* caudate nucleus, *IPL* inferior parietal lobule, *L* left hemisphere, *R* right hemisphere

thalamus as seed. A one sample *t* test on time-averaged FC maps obtained with the thalamic and the PCC/PCUN seeds, respectively, showed positive and negative correlations during nondischarge period (Fig. 9). Note that a positive correlation between the thalamus and the regions of DMN was observed during the nondischarge period (Fig. 9).

We also extracted topology measures of dynamic large-scale functional connectome across time. By means of one-way within-subject ANOVA, we found no significant change across intervals for any of the overall topology measures (e.g., small-worldness in Fig. 9c).

Discussion

In this study, we combined dynamic FC and graph theoretical analyses to explore the switching of GSWDs-related networks, as well as the whole-brain functional connectome over the different time periods during AS. We found an abnormal pattern of anti-correlation between the thalamus (thalamus network) and the PCC/PCUN (belonging to the DMN), and complex transitions of functional connectome topology over the preictal, ictal and postictal periods. These findings may contribute to a better understanding of the patho-physiological mechanisms underlying seizure initiation, maintenance and termination of AS.

Dynamic network changes of the thalamus and the DMN

The abnormal FC pattern between the thalamus and the DMN was the most remarkable finding of the present study. The FC between the thalamus and the DMN showed negative correlation during AS, which became positive in the normal physiological state (Greicius et al. 2007; Zhang et al. 2008). GSWDs-related activations in the thalamus and deactivations in the DMN are typically observed in AS, suggesting a link with GSWD generation and functional suspension during seizure (Blumenfeld 2012; Gotman et al.
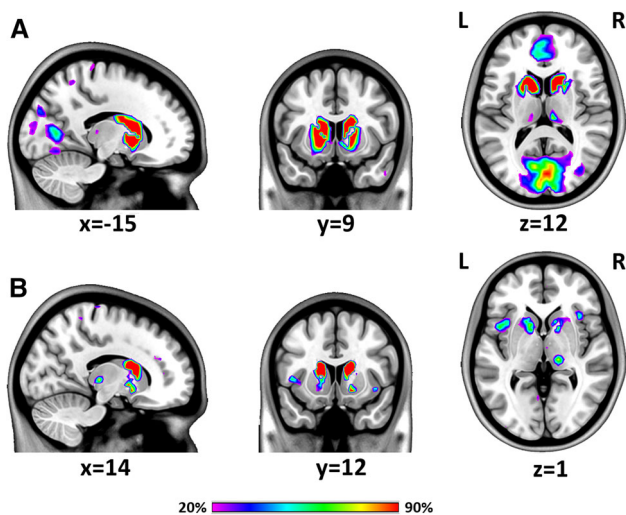
Fig. 6 Evaluation of the reliability of dynamic functional connectivity findings. The 28 seizures were divided into two groups of 14 seizures to conduct a split-half analysis, which was repeated 100 times. For each group, significant changes in the thalamus network (**a**) and in the DMN (**b**) across the preictal, ictal, and postictal intervals were obtained by a one-way within-subject ANOVA (FDR-corrected height threshold $P < 0.05$, and extent threshold $k = 5$ voxels). The brain regions with significant changes in both groups for each of the 100 iterations were combined to create a consistency map (values ranging from 20 to 90 %). These maps are represented over an anatomical template in sagittal, coronal and axial sections

2005). Importantly, this anti-correlation between the thalamus and the DMN disappeared in the later ictal and postictal periods, suggesting a dynamic recovery after a short inhibitory influence of GSWDs (from the thalamus) on the default mode of brain function (Danielson et al. 2011; Moeller et al. 2008a).

Either in the network obtained with the thalamus or the PCC/PCUN as seed, the basal ganglia (bilateral CAU and PUT) showed significant FC change during AS progression. Moreover, the basal ganglia presented similar FC transition pattern with the DMN, and reverse pattern with the thalamus. This finding suggests that the basal ganglia system, which normally maintains default function before GSWDs (Danielson et al. 2011; Moeller et al. 2008a), is transiently affected during seizure and is gradually restored to baseline connectivity afterwards. Moreover, considering the important role of the basal ganglia in the modulation of epileptic discharges generalization (Luo et al. 2012), the current results provided new evidence on the modulatory role of these structures in AS.

Dynamic topological organization of functional connectome

We for the first time investigated the dynamic changes of the whole-brain functional connectome in AS using graph

theoretical analyses. Emerging evidences from connectomic studies (Bernhardt et al. 2011; Liao et al. 2010; Vaessen et al. 2012; Vlooswijk et al. 2011; Zhang et al. 2011) have supported the heuristic view of epilepsy as a brain network disorder (Kramer and Cash 2012; Laufs 2012). In contrast to conventional brain graphs constructed over observation of several minutes (Bullmore and Bassett 2011), our findings revealed a rapid reconfiguration of the functional connectome during AS.

We observed higher total connection strength during the ictal period relative to the periods before and after seizures (Figs. 6a, 7a), indicating a relative increase in large-scale brain activity synchronization caused by GSWDs (Kramer et al. 2010; Schindler et al. 2008; Wu et al. 2006). The functional connectome in the seizure period exhibited small-world topology (Sigma). The comparison between ictal and preictal periods yielded slightly significant difference in small-worldness, which is consistent with previous electrophysiological findings (Wu et al. 2006). This result possibly indicates that networks during seizure propagation acquire larger clustering coefficients (measuring local connectedness) and path lengths (measuring overall network integration), which is roughly equal to small-worldness (Kramer and Cash 2012).

As compared to preictal and ictal periods, the postictal functional connectome dramatically reduced local connectedness and overall network integration. This may underlie an apparent shift from highly information-processing efficiency for seizure propagation to long path length cost for seizure termination. Highly network integration efficiency is related to maturation processes (Fair et al. 2009) and is modulated by dynamically changing processing demands (Sepulcre et al. 2010). Here, one can assume that a similar mechanism is used to terminate a seizure. An alternative explanation is that impaired local connectedness reflects more random configurations (Kramer et al. 2010; Schindler et al. 2008). We speculate that network randomization, associated with high local efficiency of information transfer and robustness, may be considered as a self-regulatory mechanism for seizure termination (Schindler et al. 2008).

Taken together, we found a non-monotone shift of functional network topology during seizure progression. The observed changes in small-worldness 10 s before GSWD onset may have a potential implication for seizure prediction (Mormann et al. 2007). Moreover, there was a higher small-worldness during ictal period, along with a shift to randomness during the postictal period. Our findings are not completely consistent with previous observations using EEG (Kramer et al. 2010; Schindler et al. 2008; Wu et al. 2006). As suggested by Kramer and Cash (2012), cross-modalities divergences may be resolved in the future work combining EEG and fMRI.
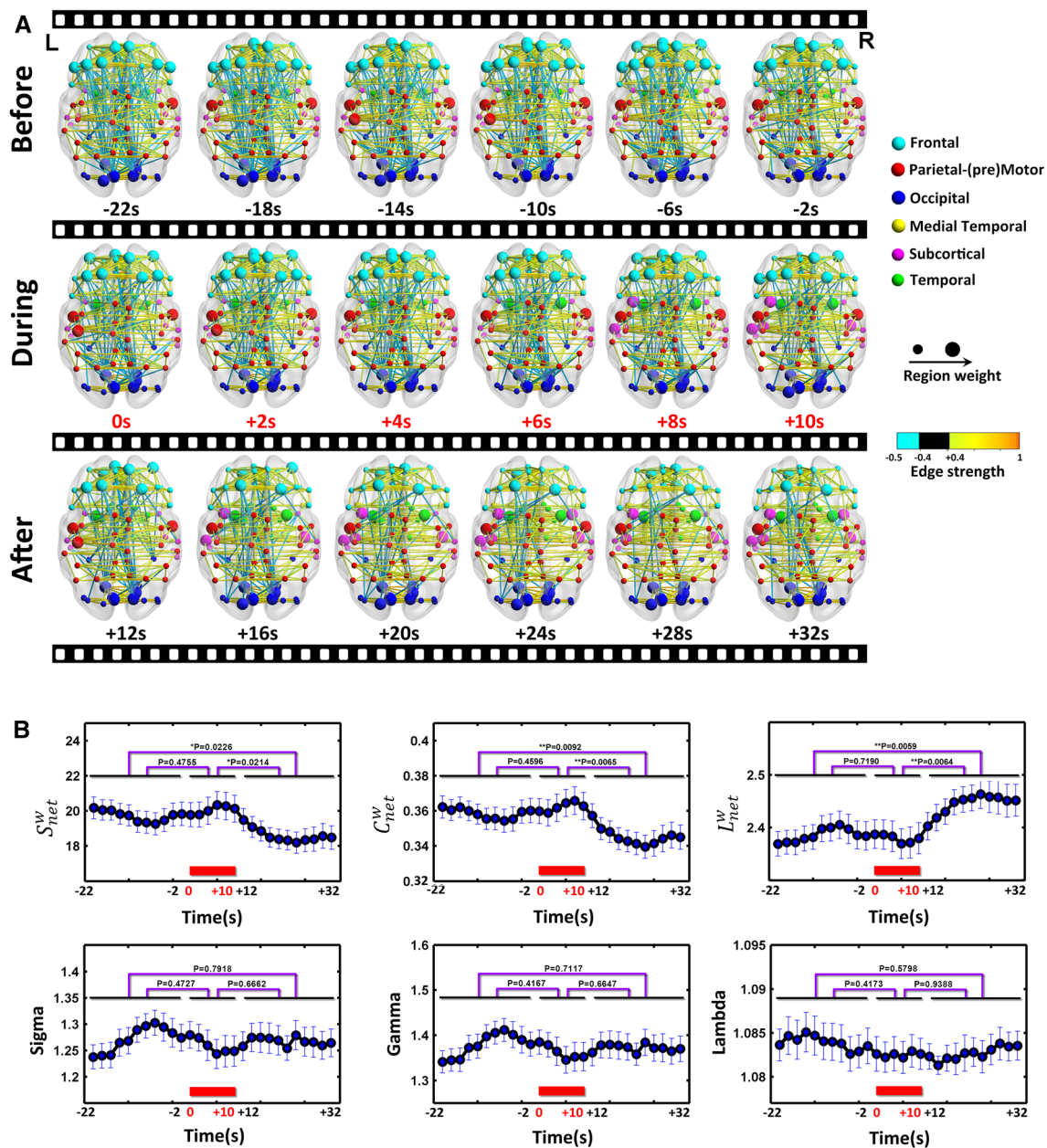
Fig. 7 Dynamic large-scale AAL-90 functional connectome during AS. **a** The large-scale AAL-90 functional connectome architecture for each interval from preictal (*Upper*), ictal (*Middle*), and postictal (*Lower*) periods are shown from −22 to +32 s (with steps of 2 s), relative to each seizure onset. Nodes are positioned according to ROIs' centroid stereotaxic coordinates and differently *colored* according to the six anatomical subsystems. Larger size nodes are hub nodes. Edges are coded according to their connection weights. **b** Overall topologies, including total connection strength in network $\left(S_{\text{net}}^{w}\right)$, overall clustering coefficient $\left(C_{\text{net}}^{w}\right)$, overall characteristic shortest path length $\left(L_{\text{net}}^{w}\right)$, small-worldness (Sigma), the normalized clustering coefficient (Gamma) and the normalized characteristic shortestpath length (Lambda), of functional connectome of each interval in three seizure periods are showed. *Error bars* represent SEM across seizures

Methodological considerations and limitations

There are still some controversies concerning optimal strategies for large-scale brain graph analysis (Bullmore and Bassett 2011). Node definition is key issue for the construction of the functional connectome. Variation of graph theoretical parameters of functional connectome might depend on the use of different prior anatomical or functional brain templates (Shirer et al. 2012; Wang et al. 2009) or on different node scales (Fornito et al. 2010; Zalesky et al. 2010). To account for this issue, we constructed a fully weighted brain network using anatomic templates with relatively low and high resolution, respectively. The connection strength (thresholded on the basis of
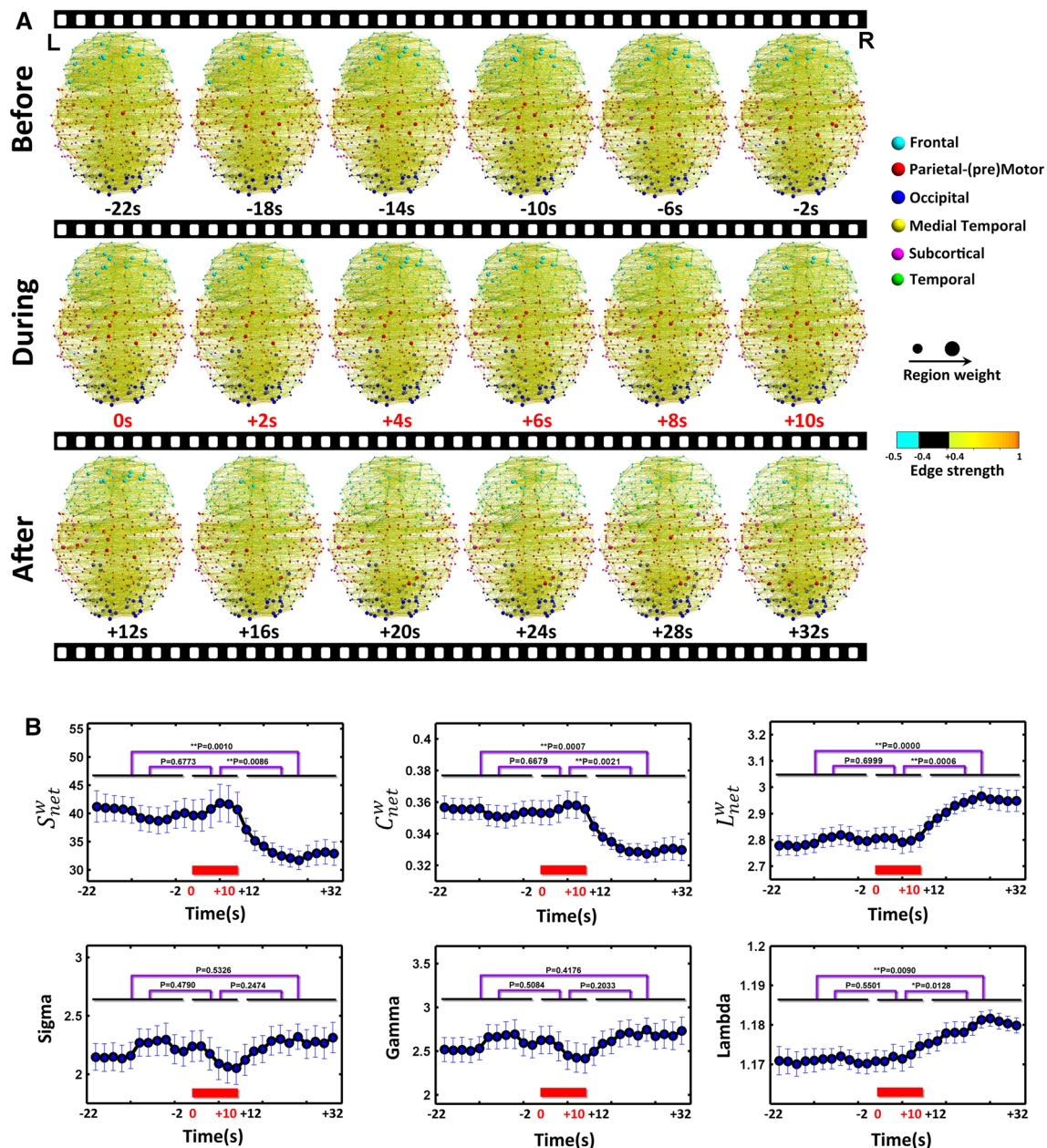
Fig. 8 Dynamic large-scale AAL-512 functional connectome during AS. **a** The large-scale AAL-512 functional connectome architecture for each interval from preictal (*Upper*), ictal (*Middle*), and postictal (*Lower*) periods are shown from −22 to +32 s (with steps of 2 s), relative to each seizure onset. Nodes are positioned according to ROIs' centroid stereotaxic coordinates and differently *colored* according to the six anatomical subsystems. Larger size nodes are hub nodes. Edges are coded according to their connection weights. **b** Overall topologies, including total connection strength in network (S_{net}^w), overall clustering coefficient (C_{net}^w), overall characteristic shortest path length (L_{net}^w), small-worldness (Sigma), the normalized clustering coefficient (Gamma) and the normalized characteristic shortestpath length (Lambda), of functional connectome of each interval in three seizure periods are showed. *Error bars* represent SEM across seizures

statistical testing with correction for multiple comparisons) in the functional connectome reflects heterogeneity in capacity and intensity of connections. Future studies using multiple cost thresholds, different brain templates or finer node scales are needed to assess consistent topological organization (Fornito et al. 2010; Zalesky et al. 2010).

To explore possible time varying dynamics, we used a sliding-window FC analysis (window length = 100 s). Since we filtered the fMRI data in a frequency band from 0.01 to 0.08 Hz, we used a window length that is the inverse of the minimum frequency (=1/0.01 Hz = 100 s) to cover a full cycle of the observed signals (Lee et al.
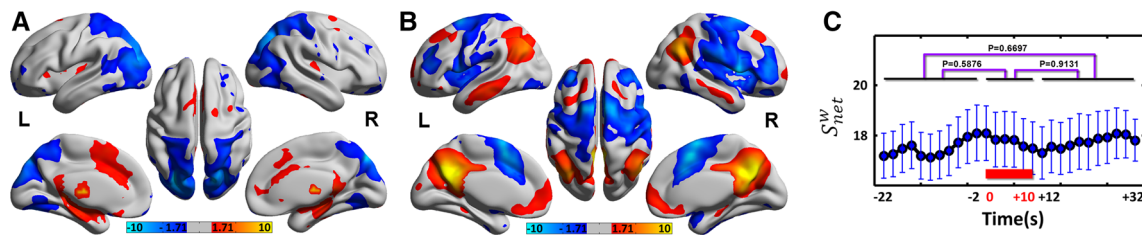
Fig. 9 Dynamic FC analysis of nondischarge state. A one sample *t* test on averaged FC maps across all intervals showed positive (*warm color*) and negative (*cool color*) correlation maps with the thalamus (**a**) and the PCC/CPUN (**b**) as seed during nondischarge state (uncorrected height threshold *P* < 0.05, and extend threshold k = 5 voxels). **c** Dynamic changes of the small-worldness of functional connectome during nondischarge state. *Error bars* represent SEM across seizures. A one-way within-subject ANOVA showed no significant difference across time periods. Note that no seizure events were present in nondischarge state, so we used seizure onset times corresponding to those detected in patients during GSWDs state

2013). We also explored the effect of other window length (60 and 200 s) on FC dynamics, which led to similar but less reliable results (Online Resource Fig. S1 and S2). Measurements over longer time window reduced the variability in functional connectivity patterns observed across the preictal, ictal and postictal stages. Shorter time windows revealed a larger spatial variance in the maps, which could however be indicative of noise or random variability. Future studies are warranted to consider various time windows for a cross-validation of FC dynamics.

Recently, it has been shown that the global signal regression, a commonly used yet controversial preprocessing step for functional connectivity analysis (Fox et al. 2009; Murphy et al. 2009; Weissenbacher et al. 2009), yields substantial increases in negative correlations (Saad et al. 2012). To check for the impact of this preprocessing step, we repeated our dynamic FC analysis without global signal regression. By doing so, we found that the main findings of the study were still preserved. Nonetheless, the distribution of functional connectivity values obtained with the thalamus as seed showed more prominent negative correlations, and it showed more prominent positive correlations when we used the PCC/PCUN as seed. In turn, the ANOVA across the preictal, ictal, and postictal intervals without global signal regression provided very similar results to those obtained by using this preprocessing step (data not shown).

A number of limitations are noteworthy. First, this study is limited by a relatively small sample size. Second, our design does not allow controlling for confounding effects of anti-epileptic drugs, which can affect normal neuronal function and produce cognitive impairments. Third, we could not evaluate whether dynamics FC are potentially related to abnormal mechanisms of consciousness in AS. Forth, our functional images were collected at standard spatial resolution, but a higher spatial resolution should be ideally pursued in a pediatric sample. Fifth, no EEG-fMRI data were acquired in matched normal children. Finally, the

dynamic FC and connectome analysis used here could not clarify whether and how brain activity involved in GSWDs propagates to other brain areas. To address this question in an animal model of AS, the 'effective connectivity' method, which refers to causal effects that one neuronal population exerts on another, has been employed (David et al. 2008). Future work using the 'effective connectivity' method in patients with AS might reveal dynamic neural correlates of seizure generation and spreading to other brain regions.

Conclusion

In conclusion, this study combined dynamic FC and graph theoretical analyses to investigate the transition of the functional connectome of the brain over the preictal, ictal and postictal periods during AS. Dynamic change of anti-correlation between the thalamus and DMN is consistent with an inhibitory effect of seizures on the default mode of brain function, which gradually fades out after seizure onset. Also, we observed complex transitions of functional network topology, implicating adaptive reconfiguration of functional brain networks. In conclusion, our work revealed novel insights into modifications in large-scale functional connectome during AS, which may contribute to a better understanding the network mechanisms of state bifurcations in epileptogenesis.

Conflict of interest All authors declare that they have no conflicts of interest.

References

Allen EA, Damaraju E, Plis SM, Erhardt EB, Eichele T, Calhoun VD (2012) Tracking whole-brain connectivity dynamics in the resting state. Cereb Cortex. doi:10.1093/cercor/bhs352

Archer JS, Abbott DF, Waites AB, Jackson GD (2003) fMRI "deactivation" of the posterior cingulate during generalized spike and wave. Neuroimage 20(4):1915–1922

Bai X, Vestal M, Berman R, Negishi M, Spann M, Vega C et al (2010) Dynamic time course of typical childhood absence seizures: EEG, behavior, and functional magnetic resonance imaging. J Neurosci 30(17):5884–5893

Bassett DS, Bullmore E (2006) Small-world brain networks. Neuroscientist 12(6):512–523

Bassett DS, Wymbs NF, Porter MA, Mucha PJ, Carlson JM, Grafton ST (2011) Dynamic reconfiguration of human brain networks during learning. Proc Natl Acad Sci USA 108(18):7641–7646

Benuzzi F, Mirandola L, Pugnaghi M, Farinelli V, Tassinari CA, Capovilla G et al (2012) Increased cortical BOLD signal anticipates generalized spike and wave discharges in adolescents and adults with idiopathic generalized epilepsies. Epilepsia 53(4):622–630

Bernhardt BC, Chen Z, He Y, Evans AC, Bernasconi N (2011) Graph-theoretical analysis reveals disrupted small-world organization of cortical thickness correlation networks in temporal lobe epilepsy. Cereb Cortex 21(9):2147–2157

Biswal B, Yetkin FZ, Haughton VM, Hyde JS (1995) Functional connectivity in the motor cortex of resting human brain using echo-planar MRI. Magn Reson Med 34(4):537–541

Blumenfeld H (2005) Cellular and network mechanisms of spike-wave seizures. Epilepsia 46(Suppl 9):21–33

Blumenfeld H (2012) Impaired consciousness in epilepsy. Lancet Neurol 11(9):814–826

Bullmore ET, Bassett DS (2011) Brain graphs: graphical models of the human brain connectome. Annu Rev Clin Psychol 7:113–140

Carney PW, Masterton RA, Harvey AS, Scheffer IE, Berkovic SF, Jackson GD (2010) The core network in absence epilepsy. Differences in cortical and thalamic BOLD response. Neurology 75(10):904–911

Carney PW, Masterton RA, Flanagan D, Berkovic SF, Jackson GD (2012) The frontal lobe in absence epilepsy: EEG-fMRI findings. Neurology 78(15):1157–1165

Chang C, Glover GH (2010) Time-frequency dynamics of resting-state brain connectivity measured with fMRI. Neuroimage 50(1):81–98

Chang BS, Lowenstein DH (2003) Epilepsy. N Engl J Med 349(13):1257–1266

Chaudhary UJ, Duncan JS, Lemieux L (2013) Mapping hemodynamic correlates of seizures using fMRI: a review. Hum Brain Mapp 34(2):447–466

Danielson NB, Guo JN, Blumenfeld H (2011) The default mode network and altered consciousness in epilepsy. Behav Neurol 24(1):55–65

David O, Guillemain I, Saillet S, Reyt S, Deransart C, Segebarth C et al (2008) Identifying neural drivers with functional MRI: an electrophysiological validation. PLoS Biol 6(12):2683–2697

de Pasquale F, Della Penna S, Snyder AZ, Lewis C, Mantini D, Marzetti L et al (2010) Temporal dynamics of spontaneous MEG activity in brain networks. Proc Natl Acad Sci USA 107(13):6040–6045

Engel J Jr, Thompson PM, Stern JM, Staba RJ, Bragin A et al (2013) Connectomics and epilepsy. Curr Opin Neurol 26(2):186–194

Fair DA, Cohen AL, Power JD, Dosenbach NU, Church JA, Miezin FM et al (2009) Functional brain networks develop from a "local to distributed" organization. PLoS Comput Biol 5(5):e1000381

Fornito A, Zalesky A, Bullmore ET (2010) Network scaling effects in graph analytic studies of human resting-state FMRI data. Front Syst Neurosci 4:22

Fornito A, Harrison BJ, Zalesky A, Simons JS (2012) Competitive and cooperative dynamics of large-scale brain functional networks supporting recollection. Proc Natl Acad Sci USA 109(31):12788–12793

Fox MD, Snyder AZ, Vincent JL, Corbetta M, Van Essen DC, Raichle ME (2005) The human brain is intrinsically organized into dynamic, anticorrelated functional networks. Proc Natl Acad Sci USA 102(27):9673–9678

Fox MD, Zhang D, Snyder AZ, Raichle ME (2009) The global signal and observed anticorrelated resting state brain networks. J Neurophysiol 101(6):3270–3283

Genovese CR, Lazar NA, Nichols T (2002) Thresholding of statistical maps in functional neuroimaging using the false discovery rate. Neuroimage 15(4):870–878

Gotman J (2008) Epileptic networks studied with EEG-fMRI. Epilepsia 49(Suppl 3):42–51

Gotman J, Grova C, Bagshaw A, Kobayashi E, Aghakhani Y, Dubeau F (2005) Generalized epileptic discharges show thalamocortical activation and suspension of the default state of the brain. Proc Natl Acad Sci USA 102(42):15236–15240

Greicius MD, Flores BH, Menon V, Glover GH, Solvason HB, Kenna H et al (2007) Resting-state functional connectivity in major depression: abnormally increased contributions from subgenual cingulate cortex and thalamus. Biol Psychiatr 62(5):429–437

Hagmann P, Cammoun L, Gigandet X, Meuli R, Honey CJ, Wedeen VJ et al (2008) Mapping the structural core of human cerebral cortex. PLoS Biol 6(7):e159

Hagmann P, Cammoun L, Gigandet X, Gerhard S, Ellen Grant P, Wedeen V et al (2010) MR connectomics: principles and challenges. J Neurosci Methods 194(1):34–45

Handwerker DA, Roopchansingh V, Gonzalez-Castillo J, Bandettini PA (2012) Periodic changes in fMRI connectivity. Neuroimage 63(3):1712–1719

He Y, Wang J, Wang L, Chen ZJ, Yan C, Yang H et al (2009) Uncovering intrinsic modular organization of spontaneous brain activity in humans. PLoS ONE 4(4):e5226

Hutchison RM, Womelsdorf T, Gati JS, Everling S, Menon RS (2012) Resting-state networks show dynamic functional connectivity in awake humans and anesthetized macaques. Hum Brain Mapp. doi:10.1002/hbm.22058

Kang J, Wang L, Yan C, Wang J, Liang X, He Y (2011) Characterizing dynamic functional connectivity in the resting brain using variable parameter regression and Kalman filtering approaches. Neuroimage 56(3):1222–1234

Killory BD, Bai X, Negishi M, Vega C, Spann MN, Vestal M et al (2011) Impaired attention and network connectivity in childhood absence epilepsy. Neuroimage 56(4):2209–2217

Kiviniemi V, Vire T, Remes J, Elseoud AA, Starck T, Tervonen O et al (2011) A sliding time-window ICA reveals spatial variability of the default mode network in time. Brain Connect 1(4):339–347

Kramer MA, Cash SS (2012) Epilepsy as a disorder of cortical network organization. Neuroscientist 18(4):360–372

Kramer MA, Eden UT, Kolaczyk ED, Zepeda R, Eskandar EN, Cash SS (2010) Coalescence and fragmentation of cortical networks during focal seizures. J Neurosci 30(30):10076–10085

Laufs H (2012) Functional imaging of seizures and epilepsy: evolution from zones to networks. Curr Opin Neurol 25(2):194–200

Lee HL, Zahneisen B, Hugger T, LeVan P, Henning J (2013) Tracking dynamic resting-state networks at higher frequencies using MR-encephalography. Neuroimage 65:216–222

Liao W, Zhang Z, Pan Z, Mantini D, Ding J, Duan X et al (2010) Altered functional connectivity and small-world in mesial temporal lobe epilepsy. PLoS ONE 5(1):e8525

Luo C, Li Q, Lai Y, Xia Y, Qin Y, Liao W et al (2011) Altered functional connectivity in default mode network in absence epilepsy: a resting-state fMRI study. Hum Brain Mapp 32(3):438–449

Luo C, Li Q, Xia Y, Lei X, Xue K, Yao Z et al (2012) Resting state basal ganglia network in idiopathic generalized epilepsy. Hum Brain Mapp 33(6):1279–1294

Moeller F, Siebner HR, Wolff S, Muhle H, Boor R, Granert O et al (2008a) Changes in activity of striato-thalamo-cortical network precede generalized spike wave discharges. Neuroimage 39(4):1839–1849

Moeller F, Siebner HR, Wolff S, Muhle H, Granert O, Jansen O et al (2008b) Simultaneous EEG-fMRI in drug-naive children with newly diagnosed absence epilepsy. Epilepsia 49(9):1510–1519

Moeller F, LeVan P, Muhle H, Stephani U, Dubeau F, Siniatchkin M et al (2010) Absence seizures: individual patterns revealed by EEG-fMRI. Epilepsia 51(10):2000–2010

Moeller F, Maneshi M, Pittau F, Gholipour T, Bellec P, Dubeau F et al (2011) Functional connectivity in patients with idiopathic generalized epilepsy. Epilepsia 52(3):515–522

Mormann F, Andrzejak RG, Elger CE, Lehnertz K (2007) Seizure prediction: the long and winding road. Brain 130(Pt 2):314–333

Murphy K, Birn RM, Handwerker DA, Jones TB, Bandettini PA (2009) The impact of global signal regression on resting state correlations: are anti-correlated networks introduced? Neuroimage 44(3):893–905

Raichle ME, MacLeod AM, Snyder AZ, Powers WJ, Gusnard DA, Shulman GL (2001) A default mode of brain function. Proc Natl Acad Sci USA 98(2):676–682

Richardson MP (2012) Large scale brain models of epilepsy: dynamics meets connectomics. J Neurol Neurosurg Psychiatry 83(12):1238–1248

Rubinov M, Sporns O (2010) Complex network measures of brain connectivity: uses and interpretations. Neuroimage 52(3):1059–1069

Saad ZS, Gotts SJ, Murphy K, Chen G, Jo HJ, Martin A et al (2012) Trouble at rest: how correlation patterns and group differences become distorted after global signal regression. Brain Connect 2(1):25–32

Salvador R, Suckling J, Coleman MR, Pickard JD, Menon D, Bullmore E (2005) Neurophysiological architecture of functional magnetic resonance images of human brain. Cereb Cortex 15(9):1332–1342

Schindler KA, Bialonski S, Horstmann MT, Elger CE, Lehnertz K (2008) Evolving functional network properties and synchronizability during human epileptic seizures. Chaos 18(3):033119

Sepulcre J, Liu H, Talukdar T, Martincorena I, Yeo BT, Buckner RL (2010) The organization of local and distant functional connectivity in the human brain. PLoS Comput Biol 6(6):e1000808

Shirer WR, Ryali S, Rykhlevskaia E, Menon V, Greicius MD (2012) Decoding subject-driven cognitive States with whole-brain connectivity patterns. Cereb Cortex 22(1):158–165

Spencer SS (2002) Neural networks in human epilepsy: evidence of and implications for treatment. Epilepsia 43(3):219–227

Sporns O (2011) The non-random brain: efficiency, economy, and complex dynamics. Front Comput Neurosci 5:5

Stefan H, Lopes da Silva FH (2013) Epileptic neuronal networks: methods of identification and clinical relevance. Front Neurol 4(8). doi:10.3389/fneur.2013.00008

Tzourio-Mazoyer N, Landeau B, Papathanassiou D, Crivello F, Etard O, Delcroix N et al (2002) Automated anatomical labeling of activations in SPM using a macroscopic anatomical parcellation of the MNI MRI single-subject brain. Neuroimage 15(1):273–289

Vaessen MJ, Jansen JF, Vlooswijk MC, Hofman PA, Majoie HJ, Aldenkamp AP et al (2012) White matter network abnormalities are associated with cognitive decline in chronic epilepsy. Cereb Cortex 22(9):2139–2147

Vlooswijk MC, Jansen JF, de Krom MC, Majoie HM, Hofman PA, Backes WH et al (2010) Functional MRI in chronic epilepsy: associations with cognitive impairment. Lancet Neurol 9(10):1018–1027

Vlooswijk MC, Vaessen MJ, Jansen JF, de Krom MC, Majoie HJ, Hofman PA et al (2011) Loss of network efficiency associated with cognitive decline in chronic epilepsy. Neurology 77(10):938–944

Wang J, Wang L, Zang Y, Yang H, Tang H, Gong Q et al (2009) Parcellation-dependent small-world brain functional networks: a resting-state fMRI study. Hum Brain Mapp 30(5):1511–1523

Weissenbacher A, Kasess C, Gerstl F, Lanzenberger R, Moser E, Windischberger C (2009) Correlations and anticorrelations in resting-state functional connectivity MRI: a quantitative comparison of preprocessing strategies. Neuroimage 47(4):1408–1416

Wu H, Li X, Guan X (2006) Networking property during epileptic seizure with multi-channel EEG recordings. In: Wang J (ed) Lecture Notes in Computer Science, vol. 3976, pp 573–578

Yang T, Luo C, Li Q, Guo Z, Liu L, Gong Q et al (2012) Altered resting-state connectivity during interictal generalized spike-wave discharges in drug-naive childhood absence epilepsy. Hum Brain Mapp. doi:10.1002/hbm.22025

Zalesky A, Fornito A, Harding IH, Cocchi L, Yucel M, Pantelis C et al (2010) Whole-brain anatomical networks: does the choice of nodes matter? Neuroimage 50(3):970–983

Zhang D, Snyder AZ, Fox MD, Sansbury MW, Shimony JS, Raichle ME (2008) Intrinsic functional relations between human cerebral cortex and thalamus. J Neurophysiol 100(4):1740–1748

Zhang Z, Liao W, Chen H, Mantini D, Ding JR, Xu Q et al (2011) Altered functional-structural coupling of large-scale brain networks in idiopathic generalized epilepsy. Brain 134(Pt 10):2912–2928

Zuo XN, Ehmke R, Mennes M, Imperati D, Castellanos FX, Sporns O et al (2012) Network centrality in the human functional connectome. Cereb Cortex 22(8):1862–1875